Supplementary Materials for

Fear Learning Enhances Neural Responses to Threat-Predictive Sensory Stimuli

Marley D. Kass†, Michelle C. Rosenthal†, Joseph Pottackal, John P. McGann

correspondence to: jmcgann@rci.rutgers.edu

†These authors contributed equally to this work.

This PDF file includes:

Materials and Methods

Animals

A total of 46 mice were used in the experiments reported here. Specifically, 14 heterozygous (n = 7) and homozygous (n = 7) OMP-spH mice (as described in (*13*,*25*, *26*)) were used for optical imaging experiments. Wild-type C57BL/6 mice (Charles River Laboratories) were used in experiments for behavioral testing (N = 21) and for respiration measurements (N = 11). All animals were adult (8-22 weeks) males and were single-housed 7 days prior to beginning experimentation to acclimate them to individual housing. Subjects were maintained in a temperature- and humidity-controlled vivarium on a 12-h light/dark cycle (lights on at 7 am), with food and water provided *ad libitum*. All experiments were conducted during the light cycle and in accordance with protocols approved by the Rutgers University Institutional Animal Care and Use Committee.

Discriminative Olfactory Fear Conditioning

Apparatus. Behavioral training and testing took place in conditioning chambers located inside ventilated and sound-attenuated isolation cubicles. During context pre-exposure and training days, the chamber floors were modular shock floors consisting of 16 metal bars that were controlled by a precision animal shocker. During behavioral testing, a separate chamber that was made distinct from the conditioning chambers by adding blue stripes to the walls and replacing the modular shock floor with a white, plastic floor was used to create a novel spatial context. The behavioral testing chamber was also equipped with a camera that was mounted inside of the isolation cubicle, providing an aerial view of the operant chamber for behavioral analysis. All chambers

were operated through programs written in Graphic State 3.03 software. A house light was turned on for the duration of each (training and testing) session. All chambers were washed before and after each session using a tergazyme (10g/L) solution followed by an ethanol (70%) solution.

Each conditioning chamber was equipped with its own custom-built olfactometer and was modified to contain a port for odor delivery (2.5 cm above the floor) and a vacuum exhaust for odor removal. The (ester) odorants methyl valerate (MV, CAS# 624-24-8, 99% purity) and *n*-butyl acetate (BA, CAS# 123-86-4, 99.5% purity) were diluted 1:200 in mineral oil and were presented at a flow rate of 1 sL/min. Steady-state concentrations of odorant stimuli were achieved across training and testing days and between subjects by calibrating the odorants daily prior to experimentation via a photoionization detector. Training and testing sessions did not begin until the olfactometer calibrations yielded odorant concentrations (reported in arbitrary units, a.u.) that peaked at 8 a.u. (see Fig. 1B, top) when measured from the center of the conditioning chamber at approximately the animal's nose height (~2.5 cm). To ensure that the odorant stimuli used during behavioral training and optical imaging sessions were matched, the same stimulus calibration procedure was used prior to imaging experiments.

Procedure. The fear conditioning paradigm is illustrated in Fig. 1A. All animals received 3 daily context pre-exposures that each consisted of a 10 min session in the conditioning chamber (without any odorant or shock stimuli being presented). Context pre-exposure was followed by a baseline imaging session and subsequent recovery day for mice used in the imaging experiment, while mice used in the behavioral and respiration experiments had 2 days of rest in the home cage (to match the study time line

across experiments). All subjects were randomly assigned to 1 of 3 groups that then underwent 3 daily sessions of fear or control training. For subjects in the Paired group, each daily training session (see Fig. 1B, bottom) began with a 180-sec acclimation period that was followed by 10 randomly-presented trials that were given at variable (140-200 sec) inter-trial intervals (ITIs). Individual trials consisted of ~15-sec odorant presentations that either co-terminated with a 0.4-mA, 0.5-sec footshock (for the CS^+ odorant, n = 5 trials; for sample trial see Fig. 1B, top) or were presented without shock (for the CS^- odorant, n = 5 trials). Two esters (MV and BA) were counterbalanced as the CS^+ and CS^- across subjects in the paired group. Daily training for subjects in the Odor Alone control group consisted of the same fear conditioning paradigm, but *without* the presentation of any shocks. Specifically, these subjects received a 180-sec acclimation period followed by 5 MV trials and 5 BA trials (~15 sec/trial) that were presented in random order at the same variable ITI per daily session. Shock Alone control training consisted of the same fear conditioning paradigm used for the paired group, but *without* the presentation of any odorants. The duration of a shock alone control training session was equivalent to that in the other groups and consisted of a shock exposure that was equivalent to that in the paired group (i.e., 5 shocks/day, but with no odorants).

Twenty-four hours after the last fear or control training session, subjects in the optical imaging experiment underwent a second imaging session; subjects in the behavioral experiment underwent behavioral testing; and subjects in the respiration experiment underwent respiratory recordings. In the behavioral study, mice were tested for odorant-evoked conditioned freezing in a novel context. This test session consisted of 1) a CS^+ trial, 2) a CS^- trial, and 3) a clean air control trial. The 3 trials were 60 sec in

duration and randomly presented at variable ITIs ranging from 4 to 6 min. Note that no shocks were presented during the test session. Additionally, while there were always 3 trials presented during the test session, the 3 trials were only comprised of 2 odor types for subjects in the shock and odor alone control groups: 1) unpaired odorants (MV and BA) and 2) clean air. Behavioral test sessions were video-recorded and analyzed offline for conditional freezing. Freezing behavior was operationalized as the absence of all visible movement save for respiration and was manually scored during each 60-sec trial via Etholog 2.2 (*27*). The raw freezing data (in sec) from each subject was then converted into percent time freezing during each 60-sec trial and analyzed across groups and trial types.

In Vivo Optical Imaging Procedures

Cranial window implantation. Surgical procedures for the implantation of chronic cranial windows were performed as described previously (*12, 13*). Briefly, mice were anesthetized with pentobarbital (10 mg/mL, 0.1 mL/10 g, i.p.) and administered additional boosters as needed to maintain deep anesthesia throughout all surgical and imaging procedures. While subjects were anesthetized, body temperature was maintained at 38 ± 0.5ºC via a feedback-regulated heating pad. A 0.1% atropine solution was administered (s.c.) to reduce nasal mucous secretions and a 0.25% bupivacaine solution was administered (s.c.) along the incision site as a local anesthetic. The scalp was removed and a custom head cap (constructed from dental acrylic) was fitted to the skull to permit replicable positioning in the head holder across imaging sessions. The skull overlying the dorsal surface of both olfactory bulbs was thinned with a handheld dental

micromotor until transparent and coated with a thin layer of clear-drying cyanoacrylate adhesive. The window was topped off with Ringer's solution and a glass coverslip during imaging procedures, and in between imaging sessions, a protective metal cover was attached to the head cap to maintain the integrity of the window.

Acquisition and analysis of odorant-evoked spH signals. *In vivo* odorant-evoked spH signals were acquired using wide-field epifluorescence imaging of the olfactory bulbs, as described previously (*13, 26, 28*). Briefly, fluorescence epi-illumination was collected with a 4× (0.28 NA) objective and illumination was provided by a 470-nm wavelength bright light-emitting diode or a 150 W xenon arc lamp with appropriate filters. Images were acquired at a pixel resolution of 256×256 and a frame rate of 7 Hz using a monochrome CCD camera.

Subjects were anesthetized, secured under the imaging apparatus, and presented with a panel of up to 5 odorants including the CS^+ and the CS^- (which were counterbalanced MV and BA), an unexposed ester (isoamyl acetate, IAA, CAS# 123-92-2), and 2 unexposed aldehydes (heptanal, HEPT, CAS# 111-71-7; hexanal, HEX, CAS# 66-25-1). To determine if the effects of emotional learning on early olfactory processing are concentration-dependent, we presented both of the training esters (i.e., MV and BA) at 3 concentrations, including 4 a.u., 8 a.u. (the training concentration), and 16 a.u. To investigate the odorant specificity of learning-induced plasticity in primary sensory representations of olfactory stimuli, we presented the other 3 unexposed/untrained odorants (i.e., IAA, HEPT, and HEX) at 8 a.u. to be comparable to the relative training concentration of the conditioning esters. Prior to daily imaging preparations, all odorant stimuli were calibrated via photoionization detection measurements, as detailed above.

All odorants were delivered through a manifold positioned ~2 cm in front of the mouse's nose via a custom vapor dilution olfactometer operated through software written in MATLAB. Each odorant stimulus was typically presented in a block of 6 individual trials that were delivered at 60-sec ITIs, with each individual trial consisting of 112 acquired frames that were comprised of a 4-sec pre-odorant baseline, 6-sec odorant presentation, and 6-sec post-odorant recovery period. Individual trials within each odor stimulus block were averaged together to improve the signal-to-noise ratio of the data. Two blocks (~6 trials/block) of blank (no odorant) trials were typically presented at the beginning and end of each imaging session, and were then averaged together and subtracted from odorant trials to correct for photobleaching.

Fluorescence imaging data were quantified and analyzed as previously reported (*13, 26, 28*). Glomerular regions of interest (ROIs) were first identified (and hand-selected) in the blank-subtracted average response maps for each concentration of each odorant stimulus. To quantify the peak odorant-evoked change in fluorescence (ΔF), spH signals for each trace corresponding to a glomerular ROI were determined by subtracting 1 sec of baseline frames (acquired during the pre-odorant baseline) from 1 sec of frames centered around the peak trace inflection after odorant onset. Because spH provides an integrative signal of exocytosis over time, the peak response magnitudes typically occurred after the end of the 6-sec odorant presentation (frames 78-84 were used for this subtraction). To evaluate potential changes in the evolution of glomerular response maps evoked by the 2 conditioning esters, we then performed 3 more subtractions and generated a time course of sub-maximal (i.e., pre-peak) response maps that were evoked throughout an odorant presentation (see Fig. S5). Specifically, we subtracted the average

of 7 baseline frames from the average of frames 1) 36-42 (1-2 sec during odorant), 2) 50-56 (3-4 sec during odorant), and 3) 64-70 (5-6 sec during odorant). SpH signals in the first second of the odorant presentation were not compared because of the low signal-to-noise ratio and to limit the influence of trial-to-trial variability in the respiratory phase at odorant onset.

All data were high-pass filtered with a Gaussian filter through software written in MATLAB and exported to Excel, SPSS 17.0, SigmaPlot 11.0, OriginPro 9.0, and Statview for statistical analysis and graphing. Hand-selected ROIs were confirmed as glomeruli receiving odorant-evoked OSN input through a statistical thresholding criterion; if a glomerulus' average response to an odorant (across trials within each block) was more than 3 standard errors (SEs) greater than 0, it was included as a response. Non-parametric statistical tests, including Kolmogorov-Smirnov (K-S), Mann-Whitney (M-W), rank sign, Friedman, and χ^2 tests, were performed to evaluate changes in populations of glomerular responses. Parametric tests, including ANOVAs and *t* tests, were used to evaluate changes in central tendencies of groups based on means from individual subjects. An α level of 0.05 was used to accept statistical significance and was Bonferroni-corrected where appropriate to correct for multiple comparisons.

Odorant-evoked ΔF values were always normalized so that we could pool data across glomeruli and mice. To determine if the effects of emotional learning were stimulus-specific, we normalized the peak evoked ΔF values relative to the maximum evoked ΔF value that was measured during pre-training imaging. This normalization was performed separately within each category of stimuli and was calculated across both pre- and post-imaging sessions per mouse. No differences in IAA-, HEPT-, and HEX-evoked

spH signals were observed between imaging sessions in any group, and thus, as intended, the responses evoked by these 3 unexposed odorants were pooled together for all subsequent analyses. The distributions of normalized peak ΔF values are shown in Fig. 2E-J.

In a separate set of analyses evaluating potential changes in the temporal evolution of CS^+- and CS^--evoked response maps during the odorant presentation, we normalized all of the pre- and post-training ΔF values per mouse relative to the maximum evoked ΔF value across all response times measured within each conditioning odorant during pre-training imaging. The distributions of these normalized ΔF values are shown in Fig. S6 and the means pooled across glomeruli are displayed in Fig. 3C. A second normalization was performed separately on each time bin to determine if the CS^+-specific enhancement of odorant-evoked nerve output varied across time during the odorant presentation. For example, each measurable ΔF value that was evoked between 1 and 2 sec of an odorant presentation during both pre- and post-training imaging sessions was divided by the maximum evoked ΔF within that bin during the pre-training imaging session, etc. These data are shown in Fig. 3D.

To generate odorant-specific concentration response functions, we normalized the peak ΔF values that were evoked by each concentration of the CS^+ and CS^- (simply MV and BA for the control groups) relative to the maximum evoked ΔF across concentrations (and within each odorant) during the pre-training imaging session. The mean concentration response functions pooled across glomeruli are shown in Fig. 4 and in Fig. S10. We also repeated this normalization for activity measured within the first time bin (pre-peak responses, Fig. S9) and generated concentration response functions for the

earliest response time that we quantified. A second normalization was performed on these data to directly compare relative changes in OSN output per concentration. As shown in Fig. 4F, peak evoked ΔF values that were evoked by each concentration of each odorant were normalized relative to the max evoked response per concentration during pre-training imaging.

The Euclidean distances (EDs) between CS^+-, CS^--, and IAA-evoked glomerular response maps were calculated on a frame-by-frame basis (1 frame = ~0.143 sec) to permit a network-level analysis for each individual mouse in the paired group. Specifically, differences among odorant-evoked glomerular response maps were quantified as EDs in *N*-dimensional vector space, where *N* was equivalent to the number of glomerular regions of interest identified in each imaging session in each mouse. Note that glomerular regions of interest included glomeruli that received odorant-evoked OSN input (per our statistical thresholding criterion) and control regions. Control regions were included in this analysis to more accurately capture the similarity-dissimilarity between overall odor representations. That is, areas of the bulb that are not receiving odorant-evoked OSN input affect the overall spatial features of a given odor map, and thus its discriminability from other odor representations. For both pre- and post-training imaging sessions, there were 6 individual ED comparisons that were made for all 3 combinations of odor maps: 1) CS^+ vs. CS^-, 2) CS^+ vs. IAA, and 3) CS^- vs. IAA. The 6 individual ED comparisons corresponded to 6 CS^+ trials, 6 CS^- trials, and 6 IAA trials that were paired up based on chronology of trial number (e.g., ED between CS^+_{t1} and CS^-_{t1}, ED between CS^+_{t2} and CS^-_{t2}, etc.). The mean±SEM ED between each pair of odor maps was calculated over the duration of the stimulus presentations for each mouse by averaging

frames within the six trial-by-trial comparisons. An example of this analysis in one mouse is shown in Fig. 3G-H and Fig. S8A-C. The network-level analysis pooled across all mice in the paired group is shown in Fig. S8D-G.

To perform odorant response selectivity analyses for the paired group, we first binarized the data per odorant. Specifically, if a ROI was statistically included as a glomerulus receiving odorant-evoked OSN input during any of the 4 time bins that we measured, then it was coded with a 1 (if not, it was coded with a 0). This binarization was first performed separately for CS^+- and CS^--evoked activity within each individual glomerulus. The binarized response profiles per glomerulus were then combined by summing across odorants, yielding 3 possible categories of response selectivity profiles: 1) CS^+-selective glomeruli (1,0); 2) CS^--selective glomeruli (0,1); and 3) non-selective (dual-responsive) glomeruli (1,1). We used this glomerular categorization to evaluate changes in response magnitudes based on odorant selectivity.

Potential structural changes (*18*) were first assessed through quantifying the frequency of glomeruli considered to be receiving OSN input during odorant presentations. In addition to changes in the absolute number of glomeruli per (PRE vs. POST) population, we considered alterations in the distributions of glomeruli within each selectivity category (Fig. 3F). Next, we quantified the odorant-evoked response size corresponding to each glomerular region of interest by totaling the number of pixels per region and converting to μm^2 to determine the glomerular response area. Under the imaging conditions detailed above, 1 pixel was equivalent to 318.87751 μm^2. The average glomerular surface response area, pooled across all (pre- and post-training)

glomerular regions of interest, was 7264.56 ± 152.04μm². These data are separated by imaging session and selectivity category and shown relative to baseline in Fig. 3E.

Respiration Recordings and Analysis

The piezosensor method was validated in a control experiment performed on a naïve, deeply-anesthetized mouse. Respiration was monitored simultaneously by a thermocouple (*28*) positioned extranasally and a force-transducing piezosensor strip positioned just below the diaphragm. The latencies of inhalation (and exhalation, not shown) onset-related events during a single respiration cycle were recorded by each method and compared across the full duration of the recordings. To further validate the piezosensor, we then demonstrated a quantitative relationship between the thermocouple- and piezosensor-generated waveforms. Average waveforms were obtained by aligning each cycle to the peak value recorded by the piezosensor. For the *n*th point of the average waveform, the value of the antiderivative at time t_n was obtained by summing the value of the antiderivative at time t_{n-1} with the product of the average waveform at t_{n-1} and the sampling rate. The initial value of the first antiderivative at time t_0 was chosen such that the area bounded by the first antiderivative and the *t*-axis was zero. The second antiderivative was multiplied by a constant to match the amplitude of the thermocouple waveform and its initial value was chosen such that its maximum and minimum values were equal to those of the thermocouple waveform. To convert to phase (in radians), each time point was then multiplied by $2\pi/T_w$, where T_w is the period of the average waveform.

In a separate experiment, mice were trained on a discriminative fear conditioning paradigm that followed the same time line and used the same counterbalanced conditioning odorants as that used for behavioral and optical imaging studies, as detailed above (Fig. 1A). Compared to that shown in Fig. 1B, modifications to the olfactometers that were connected to the conditioning chambers prior to beginning this experiment caused modest differences in the timing of odor presentations during fear training. Approximately 24 hours after the last training day, mice were anesthetized with pentobarbital (as in the imaging experiments) and underwent surgical head-mounting procedures that were comparable to those used in the imaging procedures. While mice were mounted and deeply anesthetized, respiration was then recorded during presentations of the CS^+ and CS^- odor stimuli via a piezosensor.

For post-fear conditioning respiration recordings, the CS^+ and CS^- were typically presented in blocks of 10 trials at 60-sec ITIs. Each mouse received between 8 and 60 trials of each odorant stimulus. All trials (per odorant) were then averaged together to generate overall respiration rates during CS^+ and CS^- presentations for each mouse. The piezosensor was configured such that inhalation onsets were marked by ascending zero-crossings of the output voltage trace, which was digitized (2000 Hz) and low-pass filtered (15 Hz) off-line. Individual odorant presentations were triggered by the first inhalation onset following a 60 sec ITI. In Fig. S3F-G, the instantaneous respiration rate at a given piezosensor peak was calculated as the reciprocal of the preceding inter-peak interval. All data acquisition and analysis were performed using Spike2 software.

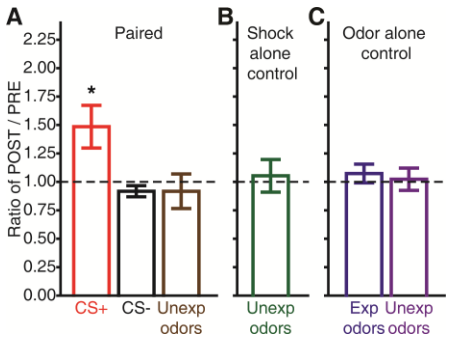

Fig. S1.

All subjects in the paired group exhibited associative, stimulus-specific neuroplasticity, whereas no plasticity was observed in shock or odor alone control groups. **(A-C)** For each mouse, glomerular responses evoked during both imaging sessions were first normalized relative to the max evoked response within each odorant category during pre-training imaging, as in Fig. 2. To quantify the overall odorant-evoked change in fluorescence (ΔF) observed in response to each odorant per mouse, individual ΔF values (corresponding to the glomeruli receiving OSN input) that were measured in response to a given odorant were then averaged together for each imaging session in each mouse. Relative changes in odorant-evoked OSN activity per mouse were assessed by dividing the post-training average ΔF value by the pre-training average ΔF value. These ratios are summarized in **A-C** as the mean±SEM group ratio of average response magnitude evoked during post-training imaging / pre-training imaging (POST / PRE) for each odor category. $*P < 0.05$ by one-sample *t* test. Number of mice (*N*) contributing to group means: paired, $N = 6$; shock alone control, $N = 4$; odor alone control, $N = 4$. Unexp, unexposed; Exp, exposed.

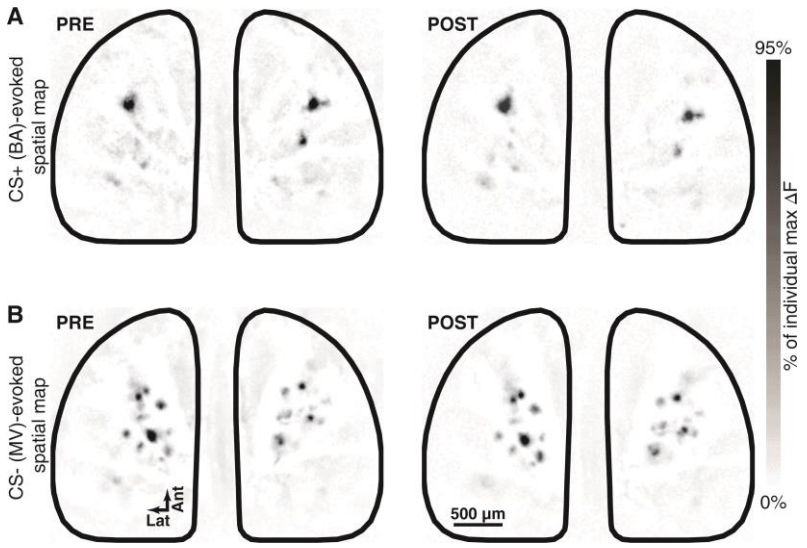

Fig. S2

The spatial arrangement of odorant-evoked glomerular response maps is unaltered by fear conditioning. **(A-B)** Glomerular response maps evoked by the CS^+ **(A)** and the CS^- **(B)** both before (left) and after (right) this representative subject underwent discriminative olfactory fear conditioning. BA, butyl acetate; MV, methyl valerate. All 4 maps are scaled relative to their individual maxima and shown in greyscale to illustrate the overall patterns of odorant-evoked activity, regardless of learning-induced changes in response magnitudes. While fear conditioning caused a ~35% increase in CS^+-evoked spH signals in this subject, there was no change in the spatial distribution of glomeruli receiving CS^+-evoked OSN input (**A**; $r = 0.811$, $P < 0.001$ by Pearson product-moment correlation coefficient). The areas receiving CS^--evoked OSN input in this subject **(B)** also remained very similar after fear conditioning ($r = 0.852$, $P < 0.001$). Note that to assess learning-induced alterations in OSN physiology, we normalized odorant-evoked glomerular response maps relative to the maximum change in fluorescence (ΔF) that was evoked during the baseline (pre-training) imaging session (as shown in Fig. 2). The range of CS^+-evoked ΔF values during the post-training imaging session exceeds that of the pre-

training imaging session (recall, CS^+-evoked spH signals became larger after fear conditioning). Thus, a consequence of imposing a single range of ΔF values (0-95% max ΔF of PRE) on both PRE and POST CS^+-evoked odor maps is a ceiling effect on the display of the pseudocolor scale for the POST map. This ceiling effect in the pseudocoloring causes the appearance of an increase in the number of CS^+-evoked glomerular responses. However, there was *no* change in the number of glomeruli receiving measurable synaptic input during presentations of the CS^+ after fear conditioning (N_{PRE} = 195, N_{POST} = 218; $P > 0.05$, by χ^2 test). If we scale each map relative to its own maximum (thus ignoring the relative enhancement of CS^+-evoked response magnitudes, as shown here in Fig. S2) we eliminate the ceiling effect and can more easily compare the overall spatial patterns of odorant-evoked activity.

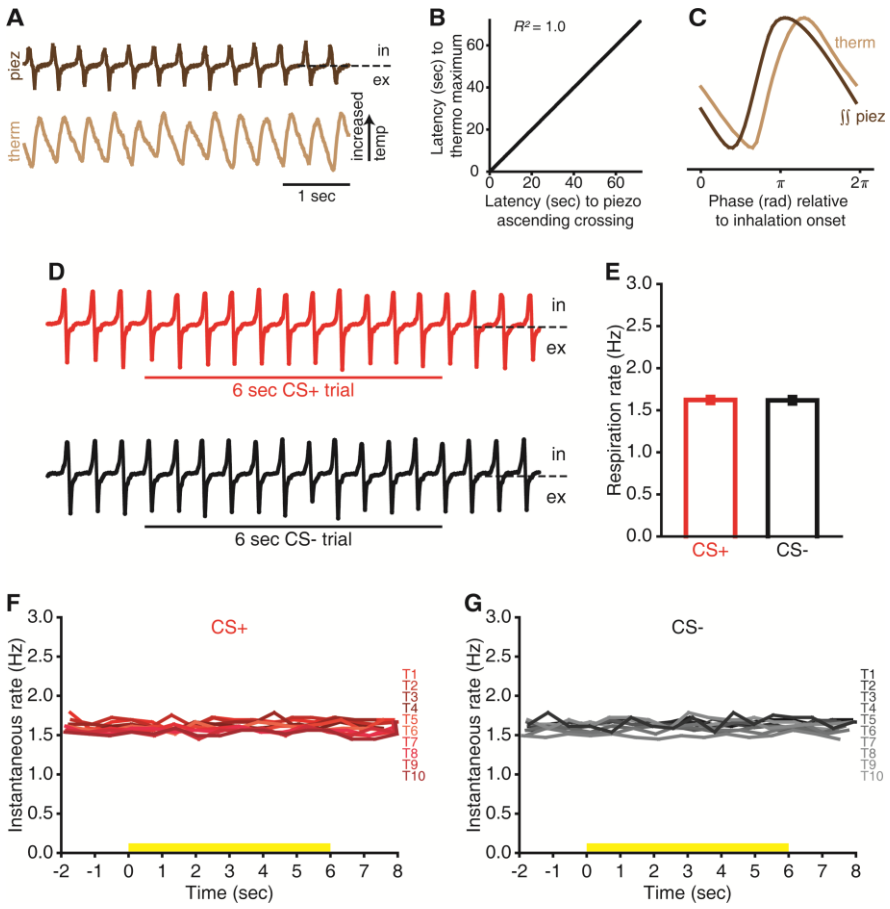

Fig. S3

Respiration does not differ during CS^+ and CS^- presentations in anesthetized mice that underwent discriminative fear conditioning. **(A)** Sample respiration traces acquired simultaneously from a naïve mouse by a piezosensor strip (brown, top) and an extranasal thermocouple (gold, bottom). The dashed line on the piezosensor trace indicates positive and negative regions of the trace, which show inhalation (in) and exhalation (ex) phases, respectively. Regions of positive slope in the thermocouple trace represent increasing temperature of extranasal air. **(B)** Latencies of inhalation onset-related events recorded simultaneously by thermocouple and piezosensor. Each point gives the latencies of the inhalation onset-related event recorded by each method during a single cycle. An analysis conducted on the exhalation onset-related events (not shown here) yielded

identical results. **(C)** Demonstration of a quantitative relationship between thermocouple- and piezosensor-generated waveforms. The average thermocouple waveform (gold) is related as a phase-shifted (lagging) scalar multiple of the second antiderivative of the average piezosensor waveform (brown). **(D)** Sample respiration traces recorded during presentations of the CS^+ (red, top) and CS^- (black, bottom) that were measured in an anesthetized preparation after this representative mouse had undergone fear conditioning. **(E)** Mean±SEM respiration rate during CS^+ and CS^- trials from 11 subjects that underwent discriminative fear conditioning. $P > 0.05$ by paired *t* test. **(F)** Instantaneous respiration rates during 10 individual trials (T1-T10) of the CS^+ (**F**, red) and the CS^- (**G**, black) from a representative mouse. The yellow bars indicate the timing of stimulus presentation. Post-fear conditioning respiration (shown in **D-G**) was monitored via a force-transducing piezosensor strip positioned just below the diaphragm.

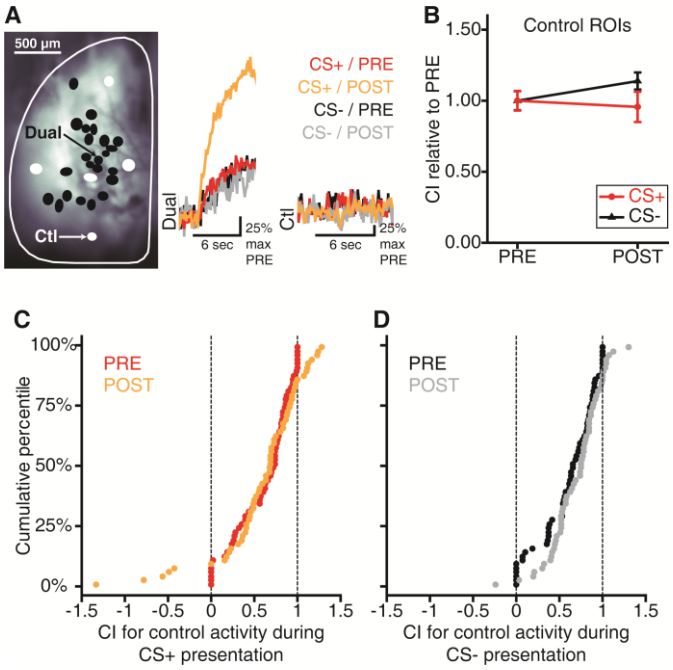

Fig. S4

The stimulus-specific enhancement of CS^+-evoked nerve output is *not* caused by odor-dependent light scatter. **(A)** Sample resting light image (RLI) from a subject in the paired group. Black circles, glomerular regions of interest (ROIs); white circles, control (Ctl) ROIs. To assess potential light scatter across the entire olfactory bulb, 5 Ctl ROIs spanning the *X* and *Y* axes of activity were selected per olfactory bulb per mouse. To determine if there were CS^+- and CS^--evoked changes in fluorescence in these Ctl regions, we then analyzed the Ctl data in the same manner as the experimental data. Example traces corresponding to the callouts shown on the RLI are displayed at right. There is an example glomerulus (Dual, left) that received input from OSNs stimulated by both the CS^+ and the CS^- during pre- and post-training imaging sessions. Although responses to both odors were observed in this glomerulus during both imaging sessions, only the CS^+-evoked response was enhanced after fear conditioning. An example Ctl ROI (Ctl, right) shows no change in fluorescence during presentations of the CS^+ and CS^- and no stimulus-specific enhancement in control activity after fear conditioning. **(B-D)**

To assess alterations in Ctl activity between pre- and post-training imaging sessions, change indexes (CIs) were calculated separately for each control ROI during CS^+ and CS^- presentations. CIs were quantified per mouse and within odorants by (Ctl ROI – min Ctl ROI value of PRE)/(max Ctl ROI of PRE – min Ctl ROI of PRE), and thus always ranged between 0 and 1 for Ctl activity measured during pre-training imaging. **(B)** Mean±SEM CIs are averaged for the CS^+ and CS^- by pooling across all Ctl ROIs from all subjects and are shown as a function of imaging session. $P > 0.05$ for odorant×imaging session interaction by 2-way, repeated measures ANOVA; $N = 60$ Ctl ROIs. **(C-D)** Cumulative probability plots showing the distribution of CIs corresponding to each individual control ROI for the CS^+ (**C**; $P > 0.05$ by K-S test) and CS^- (**D**; $P > 0.05$ by K-S test). Dashed lines indicate the min and max values during pre-training imaging.

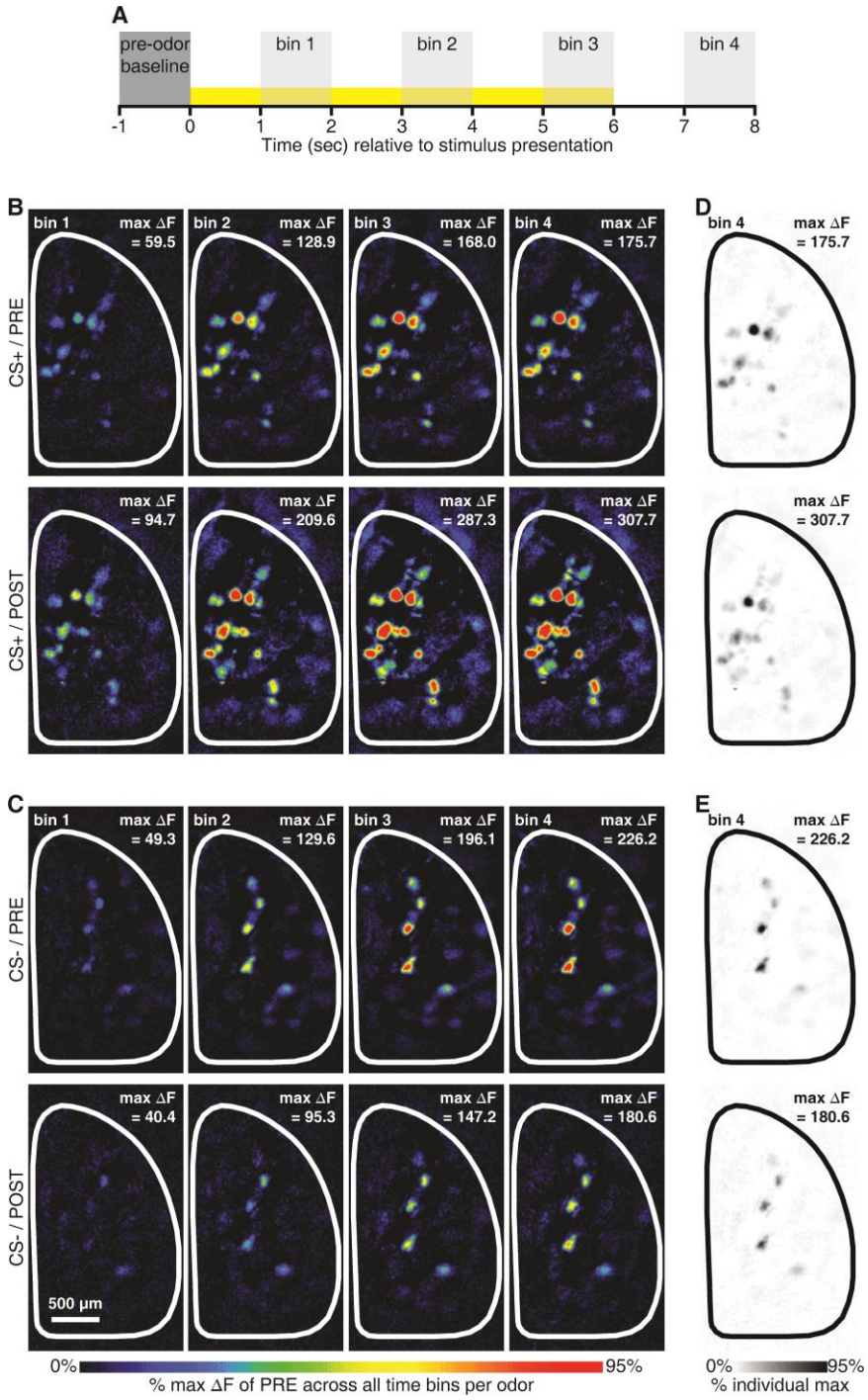

Fig. S5

Temporal evolution of CS^+- and CS^--evoked odor maps. **(A)** Timeline illustrating the 4, 1-sec time bins relative to stimulus presentation (yellow stimulus bar). One sec of baseline frames was subtracted separately from each time bin to generate difference maps

and to quantify the corresponding response magnitudes in glomeruli receiving odorant-evoked OSN input. CS^+- **(B)** and CS^-- **(C)** evoked pseudocolored difference maps measured during each time bin both before and after this subject underwent discriminative olfactory fear conditioning. CS^+- **(D)** and CS^-- **(E)** evoked maps from bin 4 are shown again in greyscale and are scaled to their individual maxima, permitting a more accurate evaluation of the similarity in the spatial arrangement of each pre- versus post-training pair of odor maps (as in Fig. S2). During this mouse's discriminative fear conditioning training, methyl valerate and butyl acetate were used as the CS^+ and CS^-, respectively.

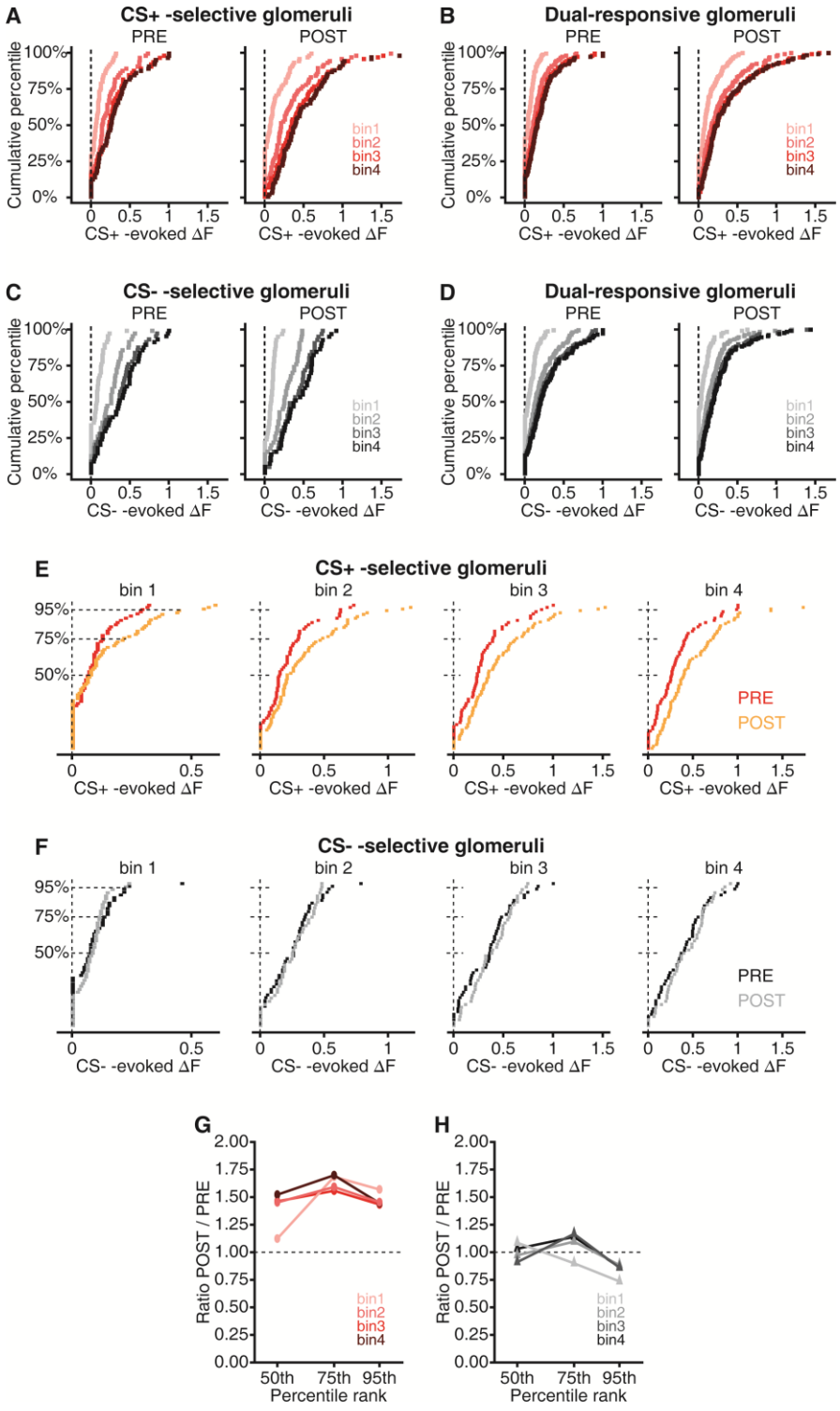

Fig. S6

Analyzing the time course of odorant-evoked spH signals. **(A-D)** Cumulative probability plots showing the distributions of odorant-evoked change in fluorescence (ΔF) values that

were measured in 4, 1-sec time bins after odor onset: 1) bin 1, 1-2 sec after odor onset; 2) bin 2, 3-4 sec after odor onset; 3) bin 3, 5-6 sec after odor onset; 4) bin 4, 7-8 sec after odor onset (corresponds with time of peak responses). CS^+- and CS^--evoked ΔFs from both imaging sessions were normalized relative to the max evoked ΔF of PRE across all 4 time bins per odorant. Panels **A-D** are separated by the 3 categories of glomerular response selectivity profiles. These categories were characterized by glomeruli that were selective for the CS^+ **(A),** selective for the CS^- **(C)**, or dual-responsive, which was the population of glomeruli receiving input from OSNs stimulated by both the CS^+ **(B)** and the CS^- **(D)**. Individual plots within each panel are separated by imaging session (PRE- and POST-training imaging). During pre-training imaging, the magnitude of CS^+- and CS^--evoked spH signals increased throughout the duration of the odorant presentations, as indicated by the rightward shifting ΔF distributions corresponding to time bins 1-4. During post-training imaging, the temporal evolution of CS^--evoked spH signals throughout the stimulus presentation was identical to that observed during the baseline session. However, CS^+-evoked spH signals that were measured in each time bin throughout the stimulus presentation were enhanced after fear conditioning. **(E-F)** Example PRE versus POST pairwise comparisons showing distributions of CS^+- and CS^--evoked ΔF values within each time bin from glomeruli that were selective for the CS^+ **(E)** or the CS^- **(F)**. The *x*-axes are truncated and expanded in plots showing PRE versus POST ΔF distributions from bins 1-3. **(G-H)** Examples showing that the learning-induced enhancement of CS^+-evoked activity was a constant proportion of the response magnitude throughout the odorant presentation. ΔF values that were ranked at the 50^{th}, 75^{th}, and 95^{th} percentiles were determined for each time bin of each session, as indicated

by the horizontal dashed lines in **E-F**. A ratio of ΔF during POST relative to ΔF during PRE was then calculated for each time bin and plotted as a function of percentile ranking for the examples of CS^+- **(G)** and CS^-- **(H)** selective glomeruli. The response distributions shown in **A**-**D** correspond to the summary plots (means±SEM) shown in Fig. 3B-C.

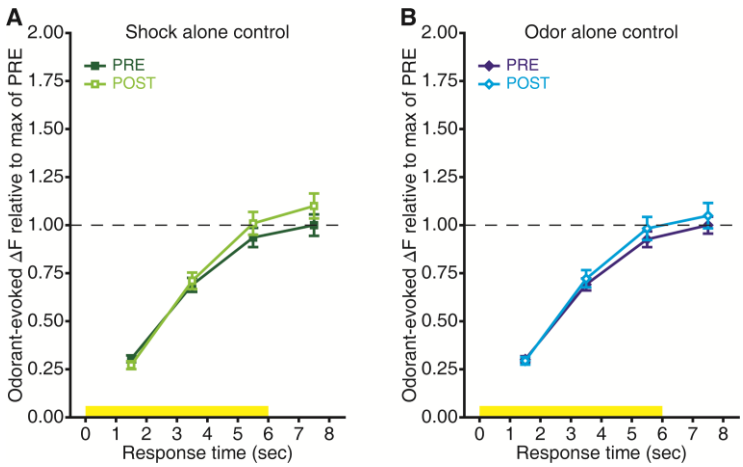

Fig. S7

The time course of responses evoked by the two conditioning odorants is not affected by shock alone or odor alone control exposures. **(A-B)** Mean±SEM change in fluorescence (ΔF) that was evoked by the 2 counterbalanced conditioning odorants shown as a function of response time relative to stimulus presentation (yellow bars). Individual ΔFs from PRE- and POST- shock alone control training **(A)** and from odor alone control training **(B)** are normalized relative to the max of baseline (dashed lines) across all response times and pooled together within each time bin. There were no odor-shock pairings during either control training protocol and thus the 2 conditioning odorants were simply unexposed and exposed stimuli for the shock alone and odor alone control groups, respectively. Number (*N*) of glomeruli contributing to data shown in **A-B**: shock alone control, N_{PRE} = 155, N_{POST} = 160; odor alone control, N_{PRE} = 195, N_{POST} = 171.

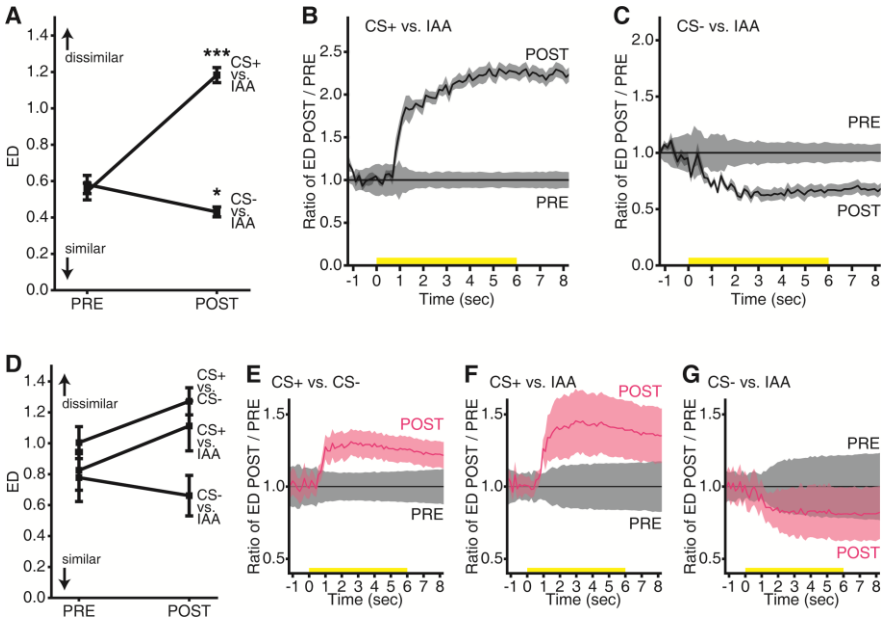

Fig. S8

Fear learning enhances the contrast between primary neural representations of a threat-predictive olfactory stimulus and other olfactory stimuli. To consider the discriminability between the overall sensory representations of the CS^+, CS^-, and IAA (an unexposed ester odorant) in each individual mouse both before and after fear conditioning, differences between odor maps were determined by Euclidean distances (EDs) in *N*-dimensional vector space, when *N* is equivalent to the number of glomerular regions of interest identified in each mouse (in each imaging session). **(A-C)** Additional results from the network-level analysis conducted on the same example mouse shown in Fig. 3G-H. **(A)** After this mouse was fear conditioned, the neural representation of the CS^+ was further in Euclidean space from the neural representation of IAA, whereas the CS^--evoked odor map became slightly more similar to the IAA-evoked odor map. EDs are summarized as means±SEM (averaged across 6 trial pairs and 0-8 sec relative to stimulus onset) and plotted as a function of imaging session. ***$P < 0.001$, *$P < 0.05$ by repeated measures ANOVA. **(B-C)** These data are normalized relative to baseline (PRE) and plotted as a

function of response time relative to stimulus presentations (yellow bar). Specifically, to analyze the relative change in ED between odor maps throughout the stimulus presentation, the mean±SEM ED (across 6 trial pairs) between CS^+- and IAA-evoked maps **(B)** and between and CS^-- and IAA-evoked maps **(C)** during the post-training imaging session was divided by that of the pre-training imaging session for each frame that was acquired. The baseline (PRE) ED between odorant-evoked response maps across trials is shown as 1.0 and the relative change in ED (POST) is plotted as a ratio of baseline. The solid traces show the mean ED across trial pairs and the shaded regions show the SEM. **(D-G)** Network level analysis averaged across 6 mice that underwent discriminative olfactory fear conditioning (includes data from example mouse shown in Fig. 3G-H and Fig. S8A-C). For each set of map comparisons, the average ED across 6 trial pairs (as in the solid traces in **B-C**) for each mouse was used to generate an overall group mean. **(D)** Group mean±SEM ED between odorant-evoked response maps before and after fear conditioning (pooled across time 0-8 sec). Group mean±SEM (solid lines ± shaded regions) ED between **(E)** CS^+ and CS^-, **(F)** CS^+ and IAA, and **(G)** CS^- and IAA sensory representations before and after fear conditioning plotted relative to baseline and as a function of time. Yellow stimulus bars indicate the time of odorant presentations.

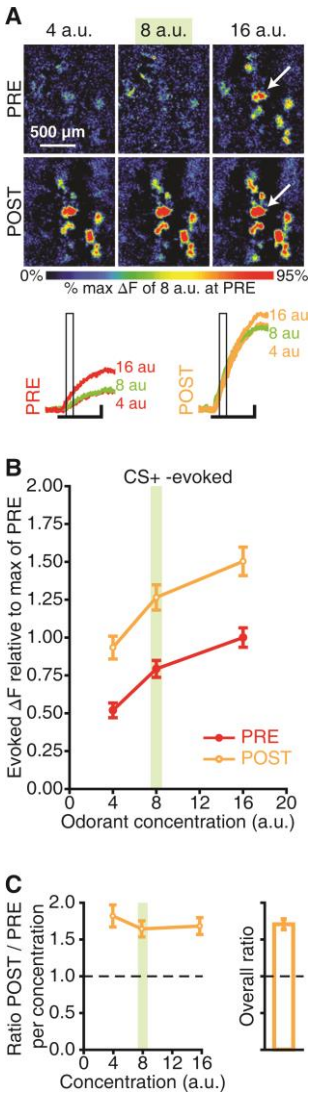

Fig. S9

Sub-maximal CS^+-evoked response amplitudes exhibit enhanced sensitivity after fear learning. This figure is analogous to Fig. 4 (which summarizes "peak" evoked spH signals that were measured during bin 4), but uses measurements taken earlier (bin 1) in the odorant presentation before the peak of the spH response. **(A)** Pseudocolored difference maps evoked by a range of concentrations (represented in arbitrary units, a.u.) centered around the training concentration (8 a.u.) of the CS^+ before (top) and after (bottom) this mouse underwent fear conditioning. During the 6-sec CS^+ presentations,

these early response maps evolved into the peak response maps shown in Fig. 4A. Example traces correspond to the callouts shown in the maps directly above. Scale bars indicate 6-sec stimulus presentations and 25% max of PRE. The boxed regions indicate the frames from bin 1 that were used to generate the corresponding early odor maps and quantify sub-maximal CS^+-evoked responses for concentration analyses shown in **B-C**. **(B)** Early (bin 1) concentration response functions evoked by the CS^+ during pre- and post-training imaging sessions. Odorant-evoked change in fluorescence (ΔF) values are normalized relative to the max evoked ΔF *across* concentrations during pre-training imaging and pooled across glomeruli (mean±SEM). **(C)** Left, early odorant-evoked ΔFs were normalized to the max evoked ΔF of PRE *within* each concentration of the CS^+ and are plotted as mean±SEM ratios to show the relative change from baseline (dashed lines) across concentrations. Right, overall ratio (pooled across all 3 concentrations) of early odorant-evoked ΔF during post-training imaging relative to pre-training imaging. Left and right plots are scaled to the same *y*-axis. The target concentration used during training is indicated in **A-C** by the color green.

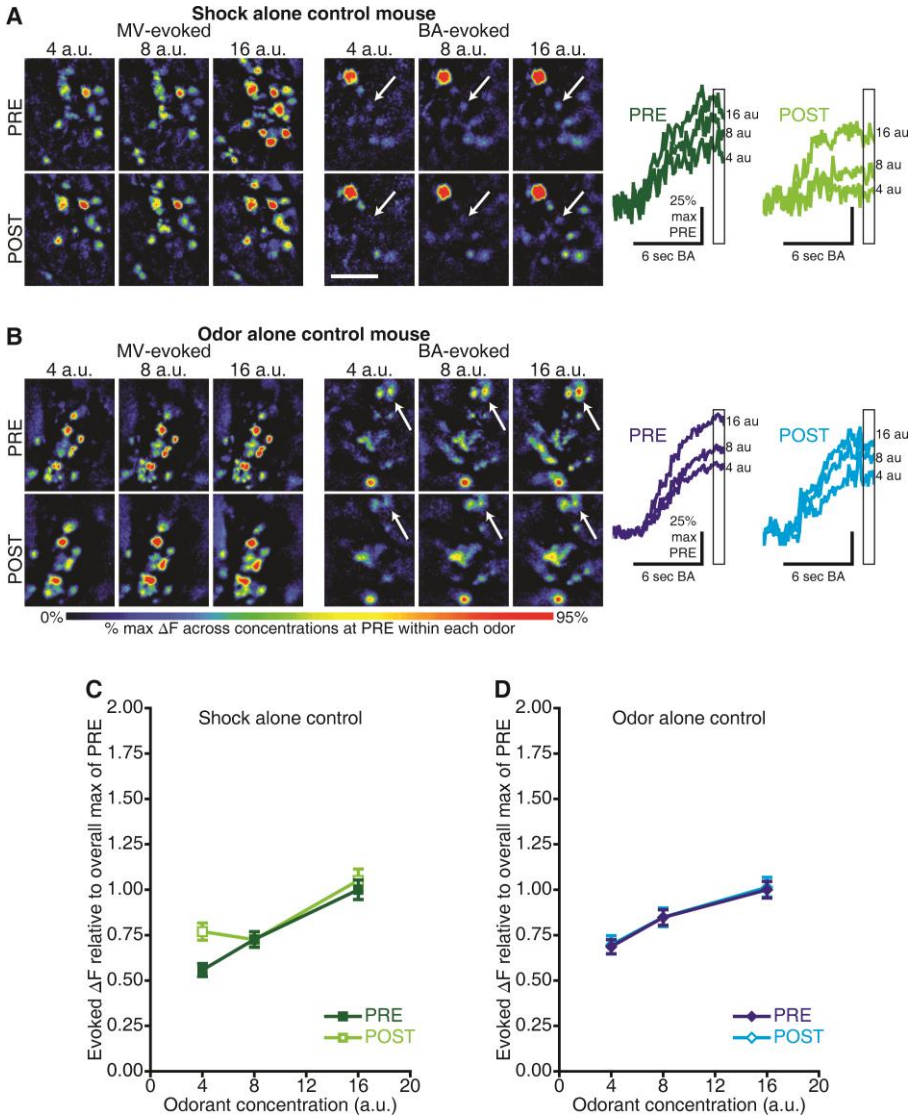

Fig. S10

Exposures to shock or odorant stimuli alone do not alter the sensitivity of OSNs stimulated by the 2 conditioning esters. For subjects that underwent shock or odor alone control training, methyl valerate (MV) and butyl acetate (BA) (the 2 counterbalanced conditioning odorants for the paired group) were simply *unexposed* or *exposed* stimuli, respectively. The concentration (in arbitrary units, a.u.) used for ester (alone) exposures was 8 a.u., paralleling that in the paired group. **(A-B)** Pseudocolored difference maps across a range of concentrations of MV and BA that were evoked both before and after

these 2 mice underwent either shock alone exposure **(A)** or odor alone exposure **(B)**. Scale bar, 500 μm. Example response amplitudes (ΔFs) corresponding to callouts in **A-B** are shown right. Boxed regions show the frames from bin 4, which were used to generate the corresponding odor maps and quantify the peak evoked glomerular responses for concentration analyses shown in **C-D**. **(C-D)** Concentration response functions evoked by the 2 conditioning esters before and after shock alone control exposure **(C)** or odor alone control exposure **(D)**. ΔFs are normalized relative to the max evoked ΔF *across* concentrations during pre-training imaging per odor, pooled across glomeruli (**C**, N_{PRE} = 163, N_{POST} = 167; **D**, N_{PRE} = 197, N_{POST} = 169), and shown as the mean±SEM.